Dissipative Particle Dynamics Simulation for Self-Assembly of Symmetric Bolaamphiphilic Molecules in Solution*)

Susumu FUJIWARA, Yoshiki IIDA, Takehide TSUTSUI, Tomoko MIZUGUCHI, Masato HASHIMOTO, Yuichi TAMURA[1)] and Hiroaki NAKAMURA[2)]

Kyoto Institute of Technology, Matsugasaki, Sakyo-ku, Kyoto 606-8585, Japan
[1)]*Konan University, 8-9-1 Okamoto, Higashinada-ku, Kobe 658-8501, Japan*
[2)]*National Institute for Fusion Science, 322-6 Oroshi-cho, Toki 509-5292, Japan*

(Received 28 December 2017 / Accepted 6 June 2018)

The self-assembly of dissolved symmetric bolaamphiphilic molecules is studied using dissipative particle dynamics simulations. Specifically, we investigate how interactions between the dual hydrophilic ends of the molecules affect the self-assembly process. Simulations show that four types of self-assembled structures (spherical micelles, tubes, vesicles, and wormlike micelles) are obtained from a random configuration of symmetric bolaamphiphilic molecules in solution. We find that the self-assembled structures change from spherical micelles to tubes, then to vesicles, and finally to wormlike micelles as the repulsive interactions between the hydrophilic ends increase. The molecular shapes in vesicles tend to be more rodlike than those in spherical micelles, tubes, or wormlike micelles.

Keywords: dissipative particle dynamics simulation, self-assembly, symmetric bolaamphiphilic molecule, spherical micelle with internal structures, tube, vesicle, wormlike micelle

DOI: 10.1585/pfr.13.3401095

1. Introduction

The study of self-organization in nonequilibrium and nonlinear systems such as plasma systems and soft-matter systems has recently attracted growing interest. Understanding the properties of self-organization that are common among these systems is extremely important to improving plasma confinement. To this end, we investigate the formation of structure in soft-matter systems, such as the formation of orientationally ordered structures in polymeric systems [1–5] and the formation of micelles and mesophases in amphiphilic molecular systems [6–13]. Amphiphilic molecules such as lipids and surfactants are composed of both hydrophilic and hydrophobic groups. In aqueous solvents, the amphiphilic molecules self-assemble spontaneously into structures such as micelles, vesicles, and lamellae [14–16]. The self-assembly of amphiphilic molecules plays a key role in several biological and industrial processes. For example, the process can be exploited to template inorganic minerals [16].

Not many simulation studies have investigated the formation of structure in bolaamphiphilic molecules. These molecules consist of a hydrophobic stalk and two hydrophilic ends. In contrast, numerous computer simulation studies have addressed the structure formation of amphiphilic molecules, which consist of a hydrophilic head group and a hydrophobic tail group. Although a few molecular simulations have been performed to investigate the formation of structure and the structural changes in a bolaamphiphilic solution [9, 12, 13, 17], little is known about the molecular-scale details of the self-assembly processes in a bolaamphiphilic solution.

This study clarifies the effect of the interaction between the hydrophilic ends of bolaamphiphilic molecules on the self-assembly process. With a view to investigating self-assembly in a symmetric bolaamphiphilic solution at the molecular level, we performed dissipative particle dynamics (DPD) simulations of symmetric bolaamphiphilic molecules in solution and analyzed the formation processes of micelles, vesicles, and other structures.

2. Simulation Model and Method

The computational model discussed below is essentially the same as that used in our previous work [13], which is based on the model of Li *et al.* [17]. A symmetric bolaamphiphilic molecule is represented as a coarse-grained flexible chain, AB_3A, which consists of a hydrophobic stalk with three particles (denoted by B) and two hydrophilic ends with one particle each (denoted by A). The solvent is modeled as hydrophilic particles (denoted by S). The mass of each particle is set to unity. The total force acting on particle i is written as the sum of the following four components, a conservative force $\boldsymbol{F}_{ij}^{\mathrm{C}}$, a dissipative force $\boldsymbol{F}_{ij}^{\mathrm{D}}$, a random force $\boldsymbol{F}_{ij}^{\mathrm{R}}$, and a harmonic spring force $\boldsymbol{F}_{ij}^{\mathrm{S}}$ which represents the stretching of the bond between neighboring particles:

author's e-mail: fujiwara@kit.ac.jp

*) This article is based on the presentation at the 26th International Toki Conference (ITC26).

$$\boldsymbol{F}_i = \sum_{j \neq i} \left(\boldsymbol{F}_{ij}^{\mathrm{C}} + \boldsymbol{F}_{ij}^{\mathrm{D}} + \boldsymbol{F}_{ij}^{\mathrm{R}} + \boldsymbol{F}_{ij}^{\mathrm{S}} \right). \tag{1}$$

The conservative force is a soft repulsion of the form

$$\boldsymbol{F}_{ij}^{\mathrm{C}} = \begin{cases} a_{ij}(1 - r_{ij})\hat{\boldsymbol{r}}_{ij} & (r_{ij} < 1) \\ 0 & (r_{ij} \geq 1) \end{cases}. \tag{2}$$

Here, a_{ij} is the maximum repulsion between particles i and j, and $\boldsymbol{r}_{ij} = \boldsymbol{r}_i - \boldsymbol{r}_j$, $r_{ij} = \left| \boldsymbol{r}_{ij} \right|$, $\hat{\boldsymbol{r}}_{ij} = \boldsymbol{r}_{ij}/r_{ij}$, where $\boldsymbol{r}_i$ is the position vector of particle i. The dissipative and random forces are, respectively, given by

$$\boldsymbol{F}_{ij}^{\mathrm{D}} = -\gamma w^{\mathrm{D}}(r_{ij})(\hat{\boldsymbol{r}}_{ij} \cdot \boldsymbol{v}_{ij})\hat{\boldsymbol{r}}_{ij}, \tag{3}$$

and

$$\boldsymbol{F}_{ij}^{\mathrm{R}} = \sigma w^{\mathrm{R}}(r_{ij})\varsigma_{ij}\Delta t^{-1/2}\hat{\boldsymbol{r}}_{ij}. \tag{4}$$

Here, w^{D} and w^{R} are weight functions that provide the range of the interactions for the dissipative and random forces, γ is the friction coefficient, σ is the noise amplitude, ς_{ij} is a Gaussian random variable with zero mean and unit variance, Δt is the time step, and $\boldsymbol{v}_{ij} = \boldsymbol{v}_i - \boldsymbol{v}_j$, where $\boldsymbol{v}_i$ is the velocity vector of particle i. An explanation for the appearance of $\Delta t^{-1/2}$ in Eq. (4) is given in Refs. [18, 19]. According to Español and Warren [18], the equilibrium distribution of the system becomes the Gibbs-Boltzmann distribution if the weight functions (w^{D} and w^{R}) and the coefficients of the dissipative and random forces (γ and σ) satisfy the following conditions:

$$w^{\mathrm{D}}(r_{ij}) = \left[w^{\mathrm{R}}(r_{ij}) \right]^2 = \begin{cases} (1 - r)^2 & (r < 1) \\ 0 & (r \geq 1) \end{cases}, \tag{5}$$

$$\sigma^2 = 2\gamma k_{\mathrm{B}} T. \tag{6}$$

These equations represent the fluctuation-dissipation theorem for the DPD method. In the present simulation, the values $\sigma = 2.4$ and $\gamma = 4.5$ are used and the temperature of the system is maintained at $k_{\mathrm{B}}T = 0.64$, where k_{B} is the Boltzmann constant. The harmonic spring force is given by

$$\boldsymbol{F}_{ij}^{\mathrm{S}} = k_{\mathrm{s}}(1 - r_{ij}/r_{\mathrm{s}})\hat{\boldsymbol{r}}_{ij}, \tag{7}$$

where k_{S} is the spring constant and r_{S} is the equilibrium bond length. The values $k_{\mathrm{S}} = 10.0$ and $r_{\mathrm{S}} = 0.86$ are used in our simulation.

Numerical integrations of the equations of motion for all particles are performed using the modified velocity Verlet algorithm [20]:

$$\begin{aligned} \boldsymbol{r}_i(t + \Delta t) &= \boldsymbol{r}_i(t) + \Delta t \boldsymbol{v}_i(t) + \tfrac{1}{2}(\Delta t)^2 \boldsymbol{F}_i(t), \\ \tilde{\boldsymbol{v}}_i(t + \Delta t) &= \boldsymbol{v}_i(t) + \lambda \Delta t\, \boldsymbol{F}_i(t), \\ \boldsymbol{F}_i(t + \Delta t) &= \boldsymbol{F}_i\left(\boldsymbol{r}(t + \Delta t), \tilde{\boldsymbol{v}}(t + \Delta t)\right), \\ \boldsymbol{v}_i(t + \Delta t) &= \boldsymbol{v}_i(t) + \tfrac{1}{2}\Delta t\, \left(\boldsymbol{F}_i(t) + \boldsymbol{F}_i(t + \Delta t)\right), \end{aligned} \tag{8}$$

where λ is a variable factor. DPD simulations with $\lambda = 0.65$ and $\Delta t = 0.04$ were carried out using the OCTA system's COGNAC engine [21]. Periodic boundary conditions were applied in all three directions. The repulsive

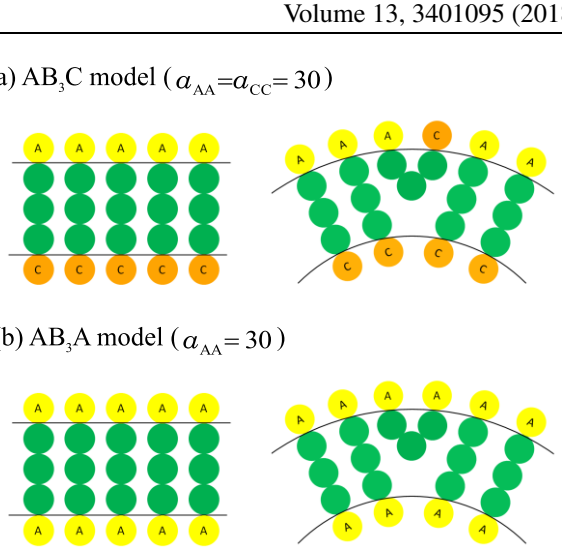

Fig. 1 Schematic illustration of a flat membrane (left) and a curved membrane (right) in (a) the AB_3C model (Ref. [13]) and (b) the present AB_3A model. Yellow and orange represent hydrophilic particles, and green represents hydrophobic particles. The hydrophobic stalk-solvent interface is represented by a thick line.

interaction parameters between the particles, a_{ij}, in Eq. (2) are given as

$$a_{ij} = \begin{pmatrix} & \mathrm{A} & \mathrm{B} & \mathrm{S} \\ \mathrm{A} & a_{\mathrm{AA}} & 200 & 25 \\ \mathrm{B} & 200 & 25 & 200 \\ \mathrm{S} & 25 & 200 & 25 \end{pmatrix}, \tag{9}$$

where a_{AA}, the repulsive interaction parameter between the hydrophilic ends, varies from 10 to 50. Note that the packing of the bolaamphiphilic molecules becomes less dense as a_{AA} increases.

The symmetric bolaamphiphilic model studied in this paper, AB_3A, differs from the previously reported asymmetric bolaamphiphilic AB_3C model in several relevant ways [13]. We here consider the cases with $a_{\mathrm{AA}} = a_{\mathrm{CC}} = 30$ in the AB_3C model and with $a_{\mathrm{AA}} = 30$ in the AB_3A model. When the bolaamphiphilic molecules form a flat membrane structure (left panels in Figs. 1 (a) and 1 (b)), the energies of the AB_3C and AB_3A models are the same. When the bolaamphiphilic molecules form a curved membrane structure by bending some constituent bolaamphiphilic molecules, *i.e.*, by changing the rodlike conformation to a U-shaped conformation (right panels in Figs. 1 (a) and 1 (b)), the models differ. The curved membrane structure in the AB_3C model is energetically unfavorable because of the large repulsion between the A and C particles. This difference suggests that the symmetric AB_3A model has the potential to form a wider variety of self-assembled structures than the asymmetric AB_3C model.

The simulations were started from a random configuration of 1000 bolaamphiphilic molecules and 40,000 solvent particles in a $24.66 \times 24.66 \times 24.66$ cubic box, which

leads to the number density of $\rho = 3.0$. We conducted DPD simulations with $t = 4.0 \times 10^4$ (1.0×10^6 time steps) for each simulation run. The self-assembly processes for various values of the repulsive interaction parameters between the hydrophilic ends, a_{AA}, are analyzed below.

3. Simulation Results and Discussion

3.1 Self-assembled structures

Figure 2 shows snapshots of the four kinds of self-assembled structures (spherical micelles with internal structures, tubes, vesicles, and wormlike micelles) that formed in our DPD simulations with various values of the repulsive interaction parameter ($a_{AA} = 15$, 25, 30, and 50). In this figure, both whole-view (left) and cross-sectional view (right) snapshots are included. The solvent particles are not shown except for those inside the tubes and vesicles in the cross-sectional view (Figs. 2 (b) and 2 (c)). The self-assembled structures that formed in our DPD simulation are listed in Table 1. This table indicates that as the repulsive interaction parameter a_{AA} increases, the spherical micelles with internal structure are replaced by tubes, then vesicles, and finally wormlike micelles.

3.2 Potential energy relaxation

Figures 3 - 6 show the total potential energy, E_{pot}, and the number of clusters that formed, n_c, for $a_{AA} = 15$, $a_{AA} = 25$, $a_{AA} = 30$, and $a_{AA} = 50$, respectively. In Fig. 3 (a), snapshots at $t = 4000$ and $t = 5000$ are also displayed for clarity. E_{pot} is defined as the sum of the potential energies associated with $\boldsymbol{F}^C_{ij}$ and $\boldsymbol{F}^S_{ij}$ as follows:

$$E_{pot} = \sum_{i<j} \left[\frac{a_{ij}}{2} \left(1 - r_{ij}\right)^2 + \frac{k_S r_S}{2} \left(1 - \frac{r_{ij}}{r_S}\right)^2 \right] \times H(1 - r_{ij}), \quad (10)$$

where $H(1 - r_{ij})$ is the Heaviside step function. The following three characteristics are demonstrated in these figures. (i) The total potential energy decreases with the decrease in the number of clusters or growth of clusters except for the case of the wormlike micelles that formed with $a_{AA} = 50$ (Fig. 6). In the case of the wormlike micelles, the potential energy is not very sensitive to the coalescence of smaller micelles into larger ones. (ii) A remarkable stepwise energy relaxation appears at $t \approx 4500$ with $a_{AA} = 15$ (Fig. 3 (a)), which suggests that large-scale coalescence of the clusters occurred. This can be clearly seen

Table 1 Self-assembled structures obtained in our simulation.

a_{AA}	Self-assembled structures
10	Spherical micelle
15	Spherical micelle
20	Tube
25	Tube, vesicle
30	Vesicle
35	Vesicle, wormlike micelle
40	Vesicle, wormlike micelle
45	Wormlike micelle
50	Wormlike micelle

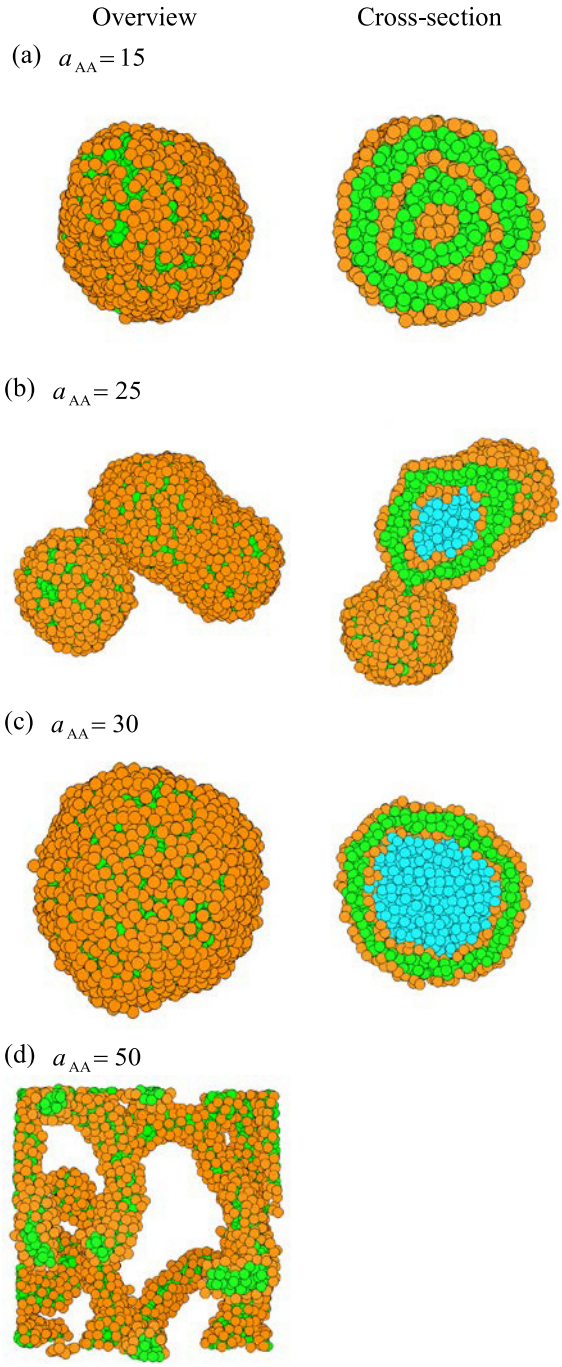

Fig. 2 Overview (left) and cross section (right) of self-assembled structures: (a) spherical micelles with internal structures at $a_{AA} = 15$, (b) tubes and vesicles at $a_{AA} = 25$, (c) vesicles at $a_{AA} = 30$, and (d) wormlike micelles at $a_{AA} = 50$. Orange, green, and light-blue particles represent the hydrophilic, hydrophobic, and solvent particles, respectively. Note that the solvent particles are not displayed except inside the tubes and vesicles in the cross-sectional view of (b) and (c).

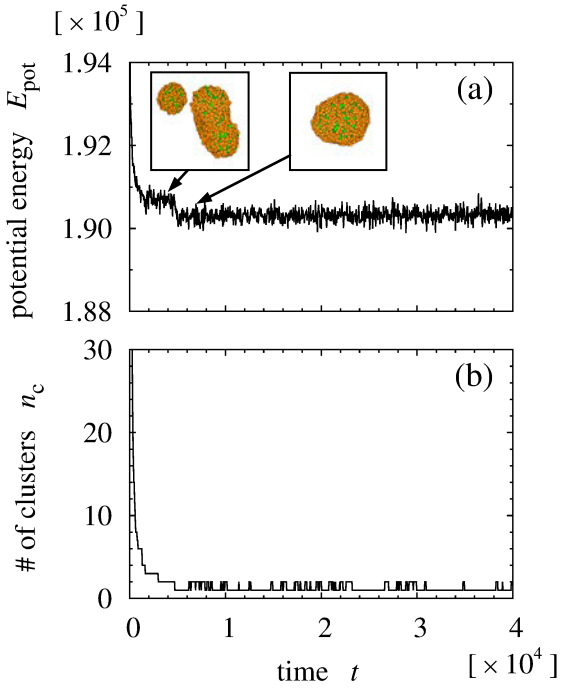

Fig. 3 Time evolution of (a) the total potential energy E_{pot} and (b) the number of clusters n_c for $\alpha_{AA} = 15$. The snapshots at $t = 4000$ and $t = 5000$ are also displayed in (a).

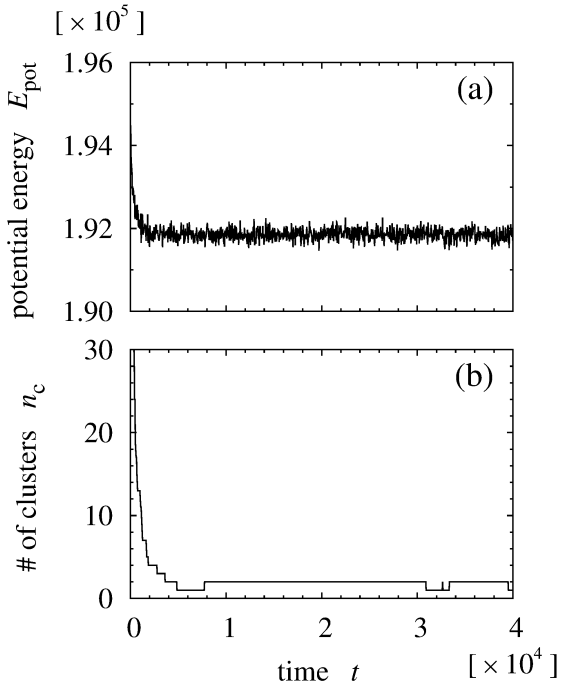

Fig. 4 Time evolution of (a) the total potential energy E_{pot} and (b) the number of clusters n_c for $a_{AA} = 25$.

from the snapshots at $t = 4000$ and $t = 5000$ shown in Fig. 3 (a). (iii) The formation of wormlike micelles takes more time (Fig. 6) than that of other self-assembled structures of spherical micelles, tubes, or vesicles (Figs. 3 - 5).

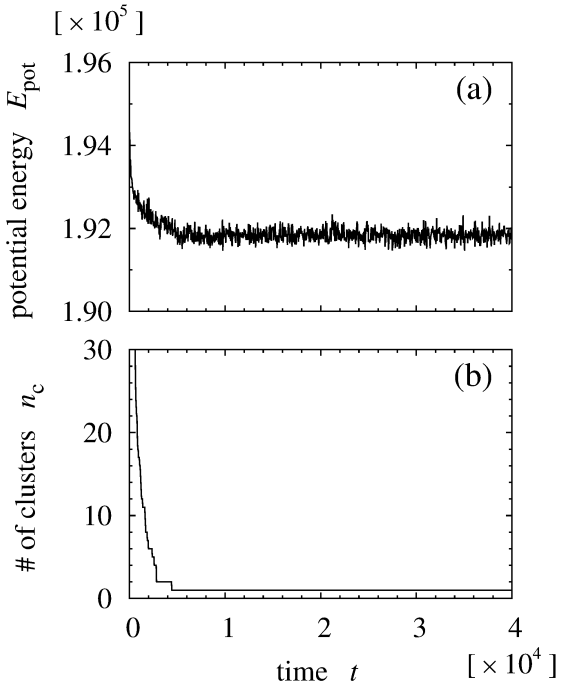

Fig. 5 Time evolution of (a) the total potential energy E_{pot} and (b) the number of clusters n_c for $a_{AA} = 30$.

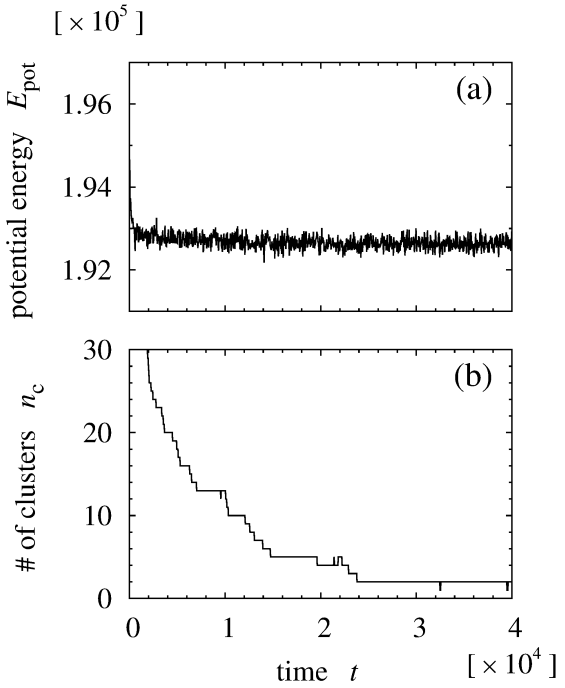

Fig. 6 Time evolution of (a) the total potential energy E_{pot} and (b) the number of clusters n_c for $a_{AA} = 50$.

3.3 Molecular shapes

To better understand the molecular shapes in the self-assembled structures, we next examine the distribution of the angles between the bond vectors of the two ends of a chain. Figure 7 shows the distribution of the cosine of the angles between the end-bond vectors along the same chain

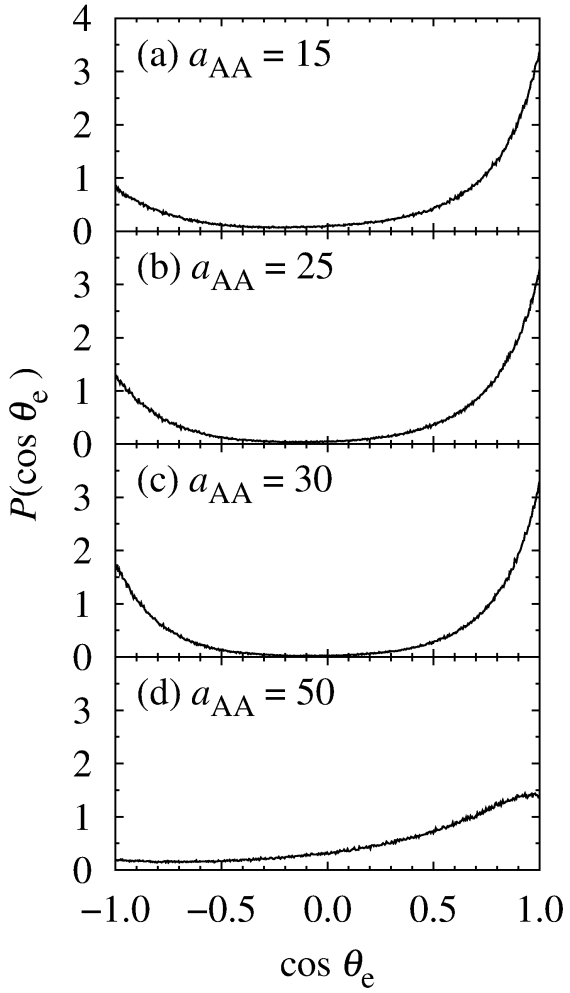

Fig. 7 Distribution function of the cosine of the angles between both end bond vectors along the same chain $P(\cos\theta_e)$ for (a) a_{AA} = 15, (b) a_{AA} = 25, (c) a_{AA} = 30, and (d) a_{AA} = 50. Note that $\cos\theta_e < 0$ corresponds to the rodlike molecules whereas $\cos\theta_e \geq 0$ corresponds to the U-shaped ones.

$P(\cos\theta_e)$ against various values of the repulsive interaction parameter (a_{AA} = 15, 25, 30, and 50). The end-bond vector is defined as the vector from B to A ($\overrightarrow{BA}$). Note that $\cos\theta_e < 0$ corresponds to rodlike molecules, and $\cos\theta_e \geq 0$ corresponds to U-shaped molecules. Figure 7 indicates that the U-shape is dominant in the self-assembled structures in all cases. The distribution function is unimodal in the case of the wormlike micelles (Fig. 7 (d)) whereas it is bimodal in the other cases (Figs. 7 (a) - 7 (c)).

Figure 8 shows the fractions of the two molecular shapes (U-shaped and rodlike) for various values of the repulsive interaction parameter a_{AA}. The molecular shapes in the vesicles (a_{AA} = 30, 35, and 40) are more rodlike than those in the other self-assembled structures.

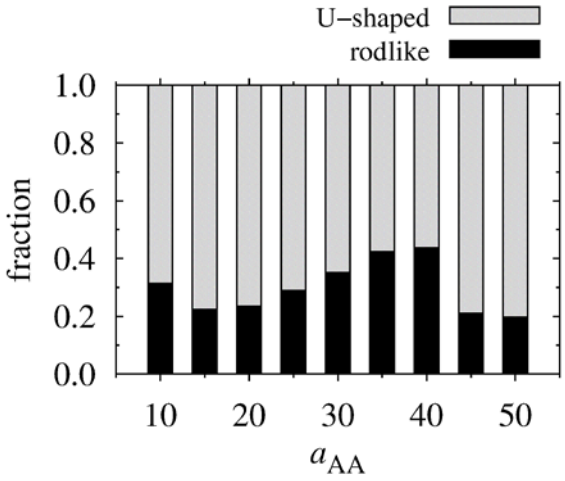

Fig. 8 Fractions of two kinds of molecular shapes (U-shaped and rodlike) versus the repulsive interaction parameter a_{AA}.

4. Conclusions

In this study, we carried out DPD simulations of symmetric flexible bolaamphiphilic molecules in solution. Our analysis of the self-assembly processes of these molecules indicated the following: (1) Four types of self-assembled structures (spherical micelles, tubes, vesicles, and wormlike micelles) form from the random configuration of symmetric bolaamphiphilic molecules in solution. (2) As the repulsive interaction parameter a_{AA} increases, the self-assembled structures change from spherical micelles to tubes, then to vesicles, and finally to wormlike micelles. (3) The fraction of rod-shaped molecules in the vesicles is relatively large than that in the other structures. (4) A greater variety of self-assembled structures are formed in the symmetric AB_3A model than in the asymmetric AB_3C model [13].

The third result shows that the molecular shape influences the self-assembled structures that form. Vesicles and tubes are composed of membrane layers. The membrane curvature of a vesicle is, on the whole, lower than that of a tube for a fixed number of constituent molecules. In the case of the symmetric bolaamphiphilic molecules, the membrane tends to be flat when more of the molecules have a rodlike shape. Therefore, vesicles form because of the smaller fraction of U-shaped molecules compared with tubes.

The fourth result indicates that molecular symmetry can affect the diversity of self-organized structures that form. This finding suggests that microscopic structure can play an important role in the self-organization of the whole system.

In the AB_3C model in Ref. [13], we discussed the self-assembled structures obtained by the DPD simulation in terms of the interaction difference of the two hydrophilic ends, $\Delta a \equiv a_{AA} - a_{CC}$. This parameter was introduced by Li *et al.* in the context of studying the shape transformations of vesicles formed from amphiphilic triblock copolymers [17]. As shown in Refs. [13, 17], Δa is an appropriate parameter for studying membranes and related structures,

so long as the relation $a_{CC} \approx 25 (= a_{CS} = a_{SS})$ holds. In the present AB_3A model, however, Δa is not a good parameter to classify the obtained self-assembled structures because the self-assembled structures are no longer membranes and do not satisfy the above relation.

Comparing the simulation results from the two models (Fig. 6 in Ref. [13] and Fig. 5 in this paper), we find that, overall, vesicles take longer to form in the AB_3C model than in the present AB_3A model regardless of the similar conditions ($a_{AA} = 30$). This suggests that the molecular structure influences the energetic balance of the self-assembly process. In the AB_3C model, the energetically unfavorable structure can be formed by neighboring A and C particles as the membrane structure forms. This situation is not possible in the AB_3A model. The energetically unfavorable structures in the AB_3C model are eliminated by flipping the molecule, and this process is quite time-consuming. This part of the process explains why, overall, vesicles take longer to form in the AB_3C model.

In future work, we plan to carry out DPD simulations of semiflexible bolaamphiphilic molecules in solution to clarify the effects of molecular rigidity on the self-assembly processes of bolaamphiphilic molecules.

Acknowledgment

This study was partially supported by JSPS KAKENHI Grant Number JP15K05244 and the NIFS Collaborative Research Program (NIFS17KNTS050).

[1] S. Fujiwara and T. Sato, J. Chem. Phys. **107**, 613 (1997).
[2] S. Fujiwara and T. Sato, J. Chem. Phys. **114**, 6455 (2001).
[3] S. Fujiwara and T. Sato, Phys. Rev. Lett. **80**, 991 (1998).
[4] S. Fujiwara and T. Sato, J. Chem. Phys. **110**, 9757 (1999).
[5] S. Fujiwara, M. Hashimoto, T. Itoh and H. Nakamura, J. Phys. Soc. Jpn. **75**, 024605 (2006).
[6] S. Fujiwara, T. Itoh, M. Hashimoto and Y. Tamura, Mol. Simul. **33**, 115 (2007).
[7] S. Fujiwara, T. Itoh, M. Hashimoto and R. Horiuchi, J. Chem. Phys. **130**, 144901 (2009).
[8] S. Fujiwara, D. Funaoka, T. Itoh and M. Hashimoto, Comput. Phys. Commun. **182**, 192 (2011).
[9] R. Shirasaki, Y. Yoshikai, H. Qian, S. Fujiwara, Y. Tamura and H. Nakamura, Plasma Fusion Res. **6**, 2401116 (2011).
[10] S. Fujiwara, M. Hashimoto, T. Itoh and R. Horiuchi, Chem. Lett. **41**, 1038 (2012).
[11] S. Fujiwara, M. Hashimoto, Y. Tamura, H. Nakamura and R. Horiuchi, Plasma Fusion Res. **9**, 3401067 (2014).
[12] S. Fujiwara, T. Miyata, M. Hashimoto, Y. Tamura, H. Nakamura and R. Horiuchi, Plasma Fusion Res. **10**, 3401029 (2015).
[13] S. Fujiwara, Y. Takahashi, H. Ikebe, T. Mizuguchi, M. Hashimoto, Y. Tamura, H. Nakamura and R. Horiuchi, Plasma Fusion Res. **11**, 2401073 (2016).
[14] J.N. Israelachvili, *Intermolecular and Surface Forces*, 2nd ed (Academic Press, London, 1992).
[15] *Micelles, Membranes, Microemulsions, and Monolayers*, edited by W.M. Gelbart, A. Ben-Shaul and D. Roux (Springer-Verlag, New York, 1994), pp. 1-104.
[16] I.W. Hamley, *Introduction to Soft Matter*, Rev. ed. (J. Wiley, Chichester, 2007).
[17] X. Li, I.V. Pivkin, H. Liang and G.E. Karniadakis, Macromolecules **42**, 3195 (2009).
[18] P. Español and P.B. Warren, Europhys. Lett. **30**, 191 (1995).
[19] R.D. Groot and P.B. Warren, J. Chem. Phys. **107**, 4423 (1997).
[20] M.P. Allen and D.J. Tildesley, *Computer Simulation of Liquids* (Clarendon, Oxford, 1987).
[21] http://octa.jp/